arXiv:1204.4287v1 [cond-mat.mes-hall] 19 Apr 2012

Calculation of the quantum conductance of silicon-doped carbon wire nanojunctions using the phase field matching theory and the tight-binding model

D. Szczęśniak[1,2], A. Khater[1], R. Szczęśniak[3], Z. Bąk[2]
1. Institute for Molecules and Materials UMR 6283,
University of Maine, Ave. Olivier Messiaen, 72085 Le Mans, France
2. Institute of Physics, Jan Długosz University in Częstochowa,
Al. Armii Krajowej 13/15, 42200 Częstochowa, Poland and
3. Institute of Physics, Częstochowa University of Technology,
*Al. Armii Krajowej 19, 42200 Częstochowa, Poland**

(Dated: March 2, 2013)

In the present work we provide the generalization of the phase field matching theory (PFMT) for the multi-scattering processes of the electronic excitations in a atomic wire nanojunctions. In the framework of the described theoretical approach, the model electronic dynamics of the considered systems are employed within the tight-binding approximation. Despite of using already determined tight-binding Hamiltonian parameters, we modify the Harrison parameters and show that covalent low-coordinated atomic wire systems can be described within the two-center approximation with a high accuracy, comparing to the first principle results. As a implementation of our model calculations, we determine the total electronic conductance of the silicon doped carbon atomic wires. The numerical analysis yields additionally the deep discussion of the propagating and evanescent fields as well as the full description of the transmission and reflection probabilities, familiar in the Landauer-Büttiker formalism. On the basis of obtained results we show that apart of the infinite periodic diatomic silicon-carbide atom wires, its finite implementations can exhibit a non-zero electronic conductance. Additionally, we discuss various non-periodic arrangements of the carbon and silicon atoms in the scattering region. In a result we note that the conductance of these purely one-dimensional nanostuctures is a strong function of its structural properties.

PACS number(s): 73.63.Nm, 73.63.-b, 03.65.Fd, 31.15.xf

I. INTRODUCTION

In nature, carbon exist in a wide range of allotopic forms. Some of them like two-dimensional graphite [1], [2] spherical fullerenes [3] or quasi-one-dimensional carbon nanotubes [4], [5] exibit exceptional physical properties and can be considered as a promising components for future nanodevices [6]. Recent discovery by Jin *et al.* [7] turns the attention on another intriguing carbon structure, namely the monatomic linear carbon wire (MLCW), which is the only stable structure among all forms of MLCW. In the experiment conducted by Jin *et al.* this purely one-dimensional carbon allotrope was produced by removing carbon atoms row by row directly from the graphene sheets. Apart of the earlier experiments on MLCW [8]-[13], method presented in [7] is the first one which allows to obtain remarkably stable freestanding MLCW.

Most often, one-dimensional atomic wires like MLCW are expected to have a various technological applications in nanoelectronics, nanomechanics, and nanomaterials *e.g.* as a interconnects between larger nanodevices [14]. Due to this fact the electronic and transport properties are the key features of these small structures [15]-[17]. However, experimental research still does not provide essential knowledge about these properties of the MLCW, and only theoretical studies shed some light.

Despite the fact that, MLCW were investigated for a long time from the theoretical point of view [18]-[29], they were obscured by the interest on other carbon structures (*i.e.* carbon nanotubes) until the beginning of the last decade. It has been shown that, from the structural point of view MLCW can undergo the formation of either cumulene (all atoms connected by double bonds) or polyyne (alternating single and triple bonds) wires [7], [20], [22], [30], [31]. However, there is no straightforward answer which of these two structures is favorable one. Experimental studies does not give any satisfying answer on this problem, while the theoretical results depends on the applied computational method. The density functional theory (DFT) calculations predicts double bond structures [32], [33] whereas *ab-initio* Hartree-Fock (HF) methods favor alternating bond systems [18]-[21], [30]. This situation arises from the fact that DFT methods tend to underestimate bond alternation (second order Jahn-Teller effect), while HF calculations overestimate it [30]. Recently however, first-principle calculations indicated, that both structures are stable, whereas cumulene presents greater stability due to the higher Gibbs free energy value [34]. Furthermore, in the work by Zhang *et al.* the cumulene was predicted to be extremely strong purely one-dimensional material along the axial direction [34].

Moreover, on the basis of the first-principle calculations the cumulene MLCW are expected to be almost perfect conductors [34]-[45], even better then a linear gold wires [32], [46], while polyyne are semiconducting [34]. This feature proves the fact that the physical properties of a given material in one-dimension may be drastically different from those in the bulk case. In particular, three-dimensional diamond structure of carbon is a good insulator, while quasi-one-dimensional carbon nanotubes can be either semiconducting or metallic. It is also worth to notice that MLCW may exibit conductance oscillations referred to the even or odd number of atoms in the wire [31], [45].

---

*Electronic address: d.szczesniak@ajd.czest.pl

In our work we would like to turn readers' attention on the problem which to our knowledge remains still unsolved, namely the behavior of the electrons in the disordered MLCW. Our interest in this issue arises from the fact that structural or chemical impurities are common in physical systems and have a significant impact on a various properties of nanomaterials [47], [48]. In particular, the foreign chemical defects injected into to the perfect structure allow to control the total conductance across the nanojunction [49].

The consequences of such disorders of defects on the electronic properties of atomic size systems are usually viewed in the terms of Landauer-Büttiker theory. Such representation allows one to connect the classical scattering theory and the conductance of the system in the framework of transmission and reflection processes. We notice that several approaches have been developed in order to calculate the transmission and reflection cross sections, where the most popular based on the first-principle calculations [50]-[53] or semi-empirical methods using the Green's function formalism [54], [55]. In the present work we investigate the scattering processes on the basis of phase field matching theory (PFMT) [56], [57] originally developed for scattering of phonons and magnons [58]. Our theoretical model rely upon the matrix calculus where the Bloch states of an ideal leads are matched to the scattering region wave functions. In this approach the electronic properties of the system are described in the framework of the tight-binding formalism, which have been previously successfully applied in the electronic transport calculations across various nanojunctions [57], [59]-[61]. In particlar, in our work we employ the appropriate Slater-Koster [62]-type Hamiltonian parameters calculated on the basis of Harrison tight-binding theory (HTBT) [63]. in this manner, the PFMT can be considered as a transparent and efficient mathematical tool for calculations of both electronic and transport properties for a wide range of atomic sized systems.

Presented work is organized in the following manner. In Sec. II, we give the detailed discussion of the model formalism which we need later on. The numerical results which incorporates propagating and evanescent electronic states for the disordered MLCW are presented in Sec. III. Finally our considerations ends with the pertinent conclusions and appropriate appendices which supplements the theoretical model presented in Sec. II.

II. THEORETICAL MODEL

A. Model dynamics

The disordered carbon atomic wire (schematic representation depicted in Fig. (1)) is described by the following tight-binding Hamiltonian block matrix

$$\mathbf{H} = \begin{pmatrix} \ddots & \cdots & 0 & 0 & \\ \vdots & \mathbf{E}_{N-1,N-1} & \mathbf{H}^{\dagger}_{N,N-1} & 0 & 0 \\ 0 & \mathbf{H}_{N,N-1} & \mathbf{E}_{N,N} & \mathbf{H}^{\dagger}_{N+1,N} & 0 \\ 0 & 0 & \mathbf{H}_{N+1,N} & \mathbf{E}_{N+1,N+1} & \vdots \\ & 0 & 0 & \cdots & \ddots \end{pmatrix}, \tag{1}$$

which is defined for overall N_x atoms in unit cell (UC) and N_l different orbitals per atom. In Eq. (1), $\mathbf{E}_{i,j}$ are the matrices composed of both diagonal ($\varepsilon_l^{n,\alpha}$) and off-diagonal ($h_{l,l',m}^{n,n',\beta}$) Hamiltonian matrix elements for N-th UC, while matrices $\mathbf{H}_{i,j}$ contains only off-diagonal elements for interactions between different UC's. Each diagonal parameter for a n-th atom in UC is characterized by the lower index l which takes the values of the angular momentum character and index α which denotes type of the atom (C or Si). The $h_{l,l',m}^{n,n',\beta}$ parameters describes the m-type bond connections ($m = \sigma$, π) between l and l' nearest-neighbour states, where index β refer to the types of interacting neighbors (C-C or Si-C). The $h_{l,l',m}^{n,n',\beta}$ matrix elements are consistent with the Slater-Koster convention [62] and expressed in the framework of Harrison's tight-binding theory (HTBT) by [63]

$$h_{l,l',m}^{n,n',\beta} = \eta_{l,l',m}\frac{\hbar^2}{m_e d_\beta^2}, \tag{2}$$

where $\eta_{l,l',m}$ are dimensionless Harrison's coefficients, m_e denotes electron vaccum mass and the d_β is the interatomic distance. Explicit forms of the $\mathbf{E}_{i,j}$ and $\mathbf{H}_{i,j}$ matrices are given in Appendix A.

In our calculations the single-particle electronic wave functions are expanded in the orthonormal basis of atomic wave functions $\phi_l(r)$ as follows

$$\Psi(r,\mathbf{k}) = \sum_{lnN} c_l(x_n - x_N, \mathbf{k})\phi_l(r - x_n - x_N). \tag{3}$$

In Eq. (3), $\mathbf{k}$ is the real wave vector, x_n denotes the position of the n-th atom in UC and x_N gives position of the UC in the atomic wire. For the ideal leads (see Fig. (1)) the wavefunction coefficients $c_l(x_n - x_N, \mathbf{k})$ in the consecutive UC's are described, in the sense of Bloch-Floquet theorem, by the following phase relation

$$c_l(x_n - x_{N+1}, \mathbf{k}) = z c_l(x_n - x_N, \mathbf{k}), \tag{4}$$

where parameter z is the phase factor of the form

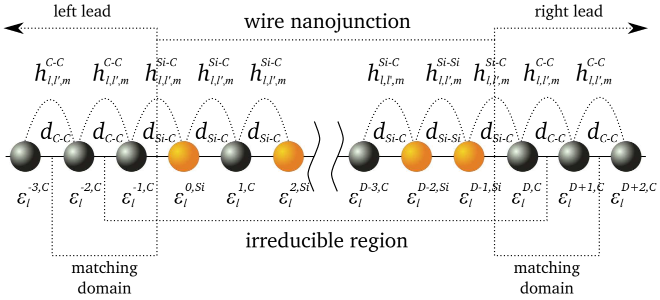
left lead
wire nanojunction
right lead
$h^{C-C}_{l,l',m}$ $h^{C-C}_{l,l',m}$ $h^{Si-C}_{l,l',m}$ $h^{Si-C}_{l,l',m}$ $h^{Si-C}_{l,l',m}$
$h^{Si-C}_{l,l',m}$ $h^{Si-Si}_{l,l',m}$ $h^{Si-C}_{l,l',m}$ $h^{C-C}_{l,l',m}$ $h^{C-C}_{l,l',m}$
d_{C-C} d_{C-C} d_{Si-C} d_{Si-C} d_{Si-C}
d_{Si-C} d_{Si-Si} d_{Si-C} d_{C-C} d_{C-C}
$\varepsilon_l^{-3,C}$ $\varepsilon_l^{-2,C}$ $\varepsilon_l^{-1,C}$ $\varepsilon_l^{0,Si}$ $\varepsilon_l^{1,C}$ $\varepsilon_l^{2,Si}$
$\varepsilon_l^{D-3,C}$ $\varepsilon_l^{D-2,Si}$ $\varepsilon_l^{D-1,Si}$ $\varepsilon_l^{D,C}$ $\varepsilon_l^{D+1,C}$ $\varepsilon_l^{D+2,C}$
irreducible region
matching domain
matching domain

FIG. 1: Schematic representation of the finite silicon doped carbon wire nanojunction between two semi-infinite quasi-onedimensional carbon leads. For the purpose of electronic transport properties we distinguish the so-called, irreducible region, and matching domains (please see section II C for more details). Moreover, the binding energies for a given atomic site and the coupling terms between neighbor atoms with corresponding interatomic distances are depicted. Please note, that in order to keep figure transparent we are omitting the n and n' indices for the coupling parameters.

$$z_{\pm} = e^{\pm i\mathbf{k}x_N}, \tag{5}$$

which corresponds to the waves propagating to the right (+) or to the left (-) direction.

In practice, the assumed orthonormal minimal basis set allows us to neglect the atomic wave functions overlap integrals, and write the $N_x \times N_l$ size eigenvalue problem for propagation waves in the following manner

$$(E\mathbf{I} - M_d)\mathbf{c}(x_N, \mathbf{k}) = 0, \tag{6}$$

where E stands for the electron eigenvalues, $\mathbf{I}$ is the identity matrix, while the dynamical matrix M_d contains Hamiltonian matrix elements and z factors. The $\mathbf{c}(x_N, \mathbf{k})$ is the $N_x \times N_l$ size vector defined as

$$\mathbf{c}(x_N, \mathbf{k}) = \begin{pmatrix} c_s(x_1 - x_N, \mathbf{k}) \\ c_{p_x}(x_1 - x_N, \mathbf{k}) \\ \vdots \\ c_l(x_n - x_N, \mathbf{k}) \end{pmatrix}. \tag{7}$$

In general, Eq. (6) gives $N_x \times N_l$ eigenvalues together with corresponding eigenvectors determines the electronic structure of the system. One can notice that the orthonormal character of the atomic orbitals may results in inadequate description of the considered electronic properties. However, what can be seen later, the proper choice of the binding energies and nearest neighbor coupling terms allows us to to obtain a very good agreement with the density functional calculations.

B. Evanescent states

The description of a disordered atomic wire is additionally supplemented by the evanescent electronic states. This situation arises from the fact that defect site breaks the perfect periodicity of the atomic wire and alters the wave functions amplitudes, what prevents proper formulation of the problem only with the use of pure Bloch factors (5).

Depending on the complexity of a given electronic state, evanescent waves are defined by the phase factors for a purely imaginary wave vectors $\mathbf{k} = i\boldsymbol{\kappa}$ as

$$z_{\pm} = e^{\mp \boldsymbol{\kappa} x_n}, \tag{8}$$

or for complex wave vectors $\mathbf{k} = \boldsymbol{\kappa}_1 + i\boldsymbol{\kappa}_2$ as

$$z_{\pm} = e^{\mp (i\boldsymbol{\kappa}_1 - \boldsymbol{\kappa}_2) x_n}. \tag{9}$$

The phase factors of the form (8) and (9) respectively defines exponential and oscillating evanescent states which both decay to the right (+) or left (-) direction. Please note that given l-type evanescent wave corresponds to the energies beyond the energy band described by the propagating wave in this state.

The functional behavior $z(E)$, for both propagating and evanescent states at given N, is described, on the basis of Eq. (4) and (6), by the generalized eigenvalue problem for z

$$\left[\begin{pmatrix} E\mathbf{I} - \mathbf{E}_{N,N} & \mathbf{H}_{N,N-1} \\ \mathbf{I} & 0 \end{pmatrix} - z \begin{pmatrix} -\mathbf{H}^{\dagger}_{N,N-1} & 0 \\ 0 & \mathbf{I} \end{pmatrix} \right] \times \begin{pmatrix} \mathbf{c}(x_N, \mathbf{k}) \\ \mathbf{c}(x_{N-1}, \mathbf{k}) \end{pmatrix} = 0, \tag{10}$$

which is twice as big as the previous eigenvalue problem of Eq.(6). In general, Eq. (10) gives $2N_xN_l$ eigenvalues as a N_xN_l pairs of z and z^{-1}. Please note, that some of the solutions are trivial or non-physical. Additionally for systems with more than one atom per UC, matrices $\mathbf{H}_{N,N-1}$ and $\mathbf{H}^{\dagger}_{N,N-1}$ are singular. In order to obtain only non-trivial solutions, eigenvalue problem (1) is reduced to the appropriate $2N_l$ size problem, by using the partitioning technique (please see Appendix B). Moreover, only solutions with $|z| = 1$ (propagating waves) and $|z| < 1$ for $\mathrm{Im}[z] = 0$ (evanescent waves) are retained as a physical ones.

C. Phase field matching theory

Let us now consider the scattering problem at the defect domain ($N \in [0, D-1]$) of the quasi one-dimensional wire nanojunction as presented in Fig. 1. In particular, the representative set of the atomic sites includes the irreducible domain which interacts with its first boundary neighbors of the left and right leads, respectively. The general concern is to calculate the wave function coefficients for each of the sites within the representative set.

The $c_l(x_n - x_N, \mathbf{k})$ coefficients of interest are described by the Eq. (6), however for the purpose of our calculations it is convenient to rewrite Eq. (6) in the terms of

Eq. (7). Hence, more familiar form of the equation of motion for a given N is expressed as

$$(E\mathbf{I} - \mathbf{E}_{N,N} - \mathbf{H}_{N,N-1} - \mathbf{H}^{\dagger}_{N,N-1})\mathbf{c}(x_N, \mathbf{k}) = 0, \quad (11)$$

Further, Eq. (11) can be written for each point in the real space which is included in the representative set of the atomic sites. This procedure generates $N_d + 2$ equations of motion of the form (11) and $N_d + 4$ corresponding and independent $\mathbf{c}(x_N, \mathbf{k})$ vectors. At this point, we notice that such set of equations cannot be solved directly, since the considered unknown wave function coefficients always outnumbered the equations of motion. Nonetheless, within the phase field matching theory, this algebraic problem can be reduced into the solvable size.

In the first step the considered problem is treated as a scattering process within the Landauer-Büttiker formalism. Assuming that the incoming wave propagates from left to right the wave function coefficients on the left and right side of the perturbed domain are written as

$$\begin{aligned} \mathbf{c}^L(x_N, \mathbf{k}) &= \mathbf{c}_l(\mathbf{k}) z^{-N} \\ &+ \sum_{l'} \mathbf{c}_{l'}(\mathbf{k}) z^N r_{l,l'} \;\; \text{for} \;\; N \leqslant -1, \end{aligned} \quad (12)$$

$$\mathbf{c}^R(x_N, \mathbf{k}) = \sum_{l'} \mathbf{c}_{l'}(\mathbf{k}) z^N t_{l,l'} \;\; \text{for} \;\; N \geqslant D, \quad (13)$$

where $\mathbf{c}_l(\mathbf{k})$ and $\mathbf{c}_{l'}(\mathbf{k})$ denotes the the eigenvectors of the dynamical matrix M_d at given energy for electrons incoming in l-state and being reflected or transmitted in l'-state respectively. These eigenvectors correspond directly to the eigenstates of the perfect leads and are calculated of the basis of Eq. (6). However, in order to consider also the evanescent states it is required to perform the computations by substituting the solutions of Eq. (10) into the Eq. (6). Finally, in the Eqs. (12) and (13), the $r_{l,l'}$ and $t_{l,l'}$ parameters are the components of Hilbert space and describe the reflection and transmission scattering processes, respectively.

Following Eq. (12) and Eq. (13), solutions of the Eq. (12) the set of the equations of motion can be completely determined in the terms of the $r_{l,l'}$ and $t_{l,l'}$ coefficients. In particular, it is possible to group the unknown $\mathbf{c}(x_N, \mathbf{k})$ vectors into the one $D+4$ size super-vector $\tilde{c}(\mathbf{k})$

$$\tilde{c}(\mathbf{k}) = \begin{pmatrix} \mathbf{c}(x_{-2}, \mathbf{k}) \\ \mathbf{c}(x_{-1}, \mathbf{k}) \\ \vdots \\ \mathbf{c}(x_D, \mathbf{k}) \\ \mathbf{c}(x_{D+1}, \mathbf{k}) \end{pmatrix}, \quad (14)$$

and reformulate its initial form (14) in the following way

$$\begin{aligned} \tilde{c}(\mathbf{k}) &= \begin{pmatrix} z^2 & 0 & \cdots & \cdots & \cdots & \cdots & 0 \\ z & 0 & & & & & \vdots \\ 0 & 1 & & & & & \vdots \\ \vdots & & \ddots & & & & \vdots \\ \vdots & & & 1 & & & \vdots \\ \vdots & & & & \ddots & & \vdots \\ \vdots & & & & & 1 & 0 \\ \vdots & & & & & 0 & z \\ 0 & \cdots & \cdots & \cdots & \cdots & 0 & z^2 \end{pmatrix} \\ &\times \begin{pmatrix} \mathbf{r}_{l,l'} \\ \mathbf{c}(x_0, \mathbf{k}) \\ \mathbf{c}(x_1, \mathbf{k}) \\ \vdots \\ \mathbf{c}(x_{D-2}, \mathbf{k}) \\ \mathbf{c}(x_{D-1}, \mathbf{k}) \\ \mathbf{t}_{l,l'} \end{pmatrix} + \begin{pmatrix} \mathbf{c}_l(\mathbf{k}) z^{-2} \\ \mathbf{c}_l(\mathbf{k}) z^{-1} \\ 0 \\ \vdots \\ 0 \end{pmatrix}. \end{aligned} \quad (15)$$

On the right hand side of the Eq. (14), the rectangular symmetric sparse matrix has the $(D+4) \times (D+2)$ size. Remaining two vectors decouple the $\mathbf{c}(\mathbf{k})$ coefficients into the scattering and incident terms, respectively. Finally, vectors $\mathbf{r}_{l,l'}$ and $\mathbf{t}_{l,l'}$ are mapped onto the reflection and transmission parameters, as

$$\mathbf{r}_{l,l'}(\mathbf{k}) = \sum_{l'} \mathbf{c}_{l'}(\mathbf{k}) r_{l,l'}, \quad (16)$$

$$\mathbf{t}_{l,l'}(\mathbf{k}) = \sum_{l'} \mathbf{c}_{l'}(\mathbf{k}) t_{l,l'}. \quad (17)$$

In a result, Eq.(15) reduces the $c_l(x_n - x_N, \mathbf{k})$ unknowns into the desirable number and allows to generate the following inhomogeneous set of equations

$$\begin{aligned} &\begin{pmatrix} \mathbf{M}_{1,1} & \mathbf{M}_{1,2} & 0 & \cdots & & \cdots & 0 \\ \mathbf{M}_{2,1} & \mathbf{M}_{2,2} & \ddots & \ddots & & & \vdots \\ 0 & \ddots & \ddots & \ddots & & \ddots & \vdots \\ \vdots & \ddots & \ddots & \ddots & & \ddots & 0 \\ \vdots & & \ddots & \ddots & & \mathbf{M}_{D+1,D+1} & \mathbf{M}_{D+1,D+2} \\ 0 & \cdots & \cdots & 0 & & \mathbf{M}_{D+2,D+1} & \mathbf{M}_{D+2,D+2} \end{pmatrix} \\ &\times \begin{pmatrix} \mathbf{r}_{l,l'} \\ \mathbf{c}(x_0, \mathbf{k}) \\ \mathbf{c}(x_1, \mathbf{k}) \\ \vdots \\ \mathbf{c}(x_{D-2}, \mathbf{k}) \\ \mathbf{c}(x_{D-1}, \mathbf{k}) \\ \mathbf{t}_{l,l'} \end{pmatrix} = - \begin{pmatrix} M_1^{in} \\ M_2^{in} \\ 0 \\ \vdots \\ 0 \end{pmatrix} \end{aligned} \quad (18)$$

where block matrices $M_{i,j}$ are composed of the Hamiltonian matrix elements and corresponding phase factors. Moreover, vector which incorporates the M_1^{in} and M_2^{in} elements, regroups the inhomogeneous terms of the incident wave. The explicit forms of the $M_{i,j}$ and $M_{i,j}^{in}$ components are presented in Appendix C.

In practice, Eq. (18) can be solved using standard numerical procedures, yielding the $c_l(x_n - x_N, \mathbf{k})$ coefficients inside the defect region ($N \in [0, D-1]$), and $2L$ reflection $r_{l,l'}(E)$ and transmission $t_{l,l'}(E)$ energy dependent coefficients.

We remind the fact that the transport processes in the Landauer-Büttiker theory are presented within the scattering matrix formulation. The elements of such matrix are respectively the reflection $R_{l,l'}(E)$ and transmission $T_{l,l'}(E)$ probabilities, which can be determined on the basis of $r_{l,l'}(E)$ and $t_{l,l'}(E)$ coefficients. However, it is required to normalize these coefficients with the respect to their group velocities (v_l) in order to obtain the unitarity of the scattering matrix. In what follows, the reflection and transmission probabilities are written as

$$R_{l,l'}(E) = \frac{v_{l'}}{v_l} \left| r_{l,l'}(E) \right|^2 , \tag{19}$$

$$T_{l,l'}(E) = \frac{v_{l'}}{v_l} \left| t_{l,l'}(E) \right|^2 , \tag{20}$$

where v_l denotes group velocities of the waves incoming in state l, whereas the $v_{l'}$ are the group velocities of the waves reflected or transmitted in channel l'. Discussed v_l parameters of a given l state are calculated on the basis of the altered dynamical matrix (please see Appendix D for the details). In addition, we note that for the evanescent states, group velocities are set to zero. This indicates the fact that evanescent waves do not contribute to the electronic transport, nevertheless they are required for the complete description of the multi-scattering processes.

Further, using expressions (21) and (22) the reflection probability for a wave incoming in a l-channel ($R_l(E)$) and the total reflection at the defect region ($R(E)$), respectively, are given by

$$R_l(E) = \sum_{l'} R_{l,l'}(E) \quad \text{and} \quad R(E) = \sum_{l} R_l(E). \tag{21}$$

Similarly, by summing over the output and then input channels the corresponding transmission probabilities, $T_l(E)$ and $T(E)$, can be written as

$$T_l(E) = \sum_{l'} T_{l,l'}(E) \quad \text{and} \quad T(E) = \sum_{l} T_l(E). \tag{22}$$

The $T_l(E)$ and $T(E)$ probabilities are very important in the discussion of the scattering processes since they directly correspond to the experimentally measurable observable. Likewise, the total transmission $T(E)$ allows to calculate the overall electronic conductance. In this work we assume the zero bias limit and write the total conductance in the following way

$$G(E_F) = G_0 T(E_F), \tag{23}$$

In Eq. (23), G_0 is the conductance quantum and equals $2e^2/h$. Due to the Fermi-Dirac distribution the $G(E_F)$ is calculated at the Femi energy of the perfect leads band structure, since electrons at this level give the only important contribution to the electronic conductance. Itself the Fermi energy can be determined using various methods. In the present work, the E_F value is given on the basis of the density of states calculations. For a computational details please see Appendix E.

III. NUMERICAL RESULTS AND DISCUSSION

A. The tight binding model and basic electronic properties

In this section we present the electronic structure calculations which allow us to establish our choice of tight-binding parameters and check its possible applications to the considered wire nanojunctions. The correctness of our results is validated by the comparison with the first-principles results after [32], [64].

In the first step of electronic structure calculations within the tight binding approximation, it is desirable to carefully choose the correct minimal basis set of the atomic wave functions. We note, that usually carbon is characterized by the $2s$ and $2p$ valence orbitals, wheres silicon by the $3s$ and $3p$ atomic wave function types. Such scheme is assumed in our calculations and gives us four different orbitals types (namely s, p_x, p_y and p_z) for each type of the atom. Additionally, as we already stated in Sec. II A, the described set of atomic orbitals is assumed to be of orthonormal character. However, in contrast to our choice, the electronic and transport properties of the nanoscale systems are usually described in the framework of the sophisticated non-orthogonal tight binding methods. In our opinion, such tight binding models may artificially complicate the calculations in the case of the low-coordinated systems like mono- or di-atomic wire nanojunctions. On the basis of other experimental and theoretical studies one can easily notice that the atomic wires have relatively simple structural and electronic characteristics. These facts proves, that for the calculations of electronic and transport properties of discussed atomic wires it is reasonable to consider the orthonormal rather then non-orthogonal tight binding model.

In our case the electronic states of the considered nanojunctions are described in the framework of the tight binding approach proposed by Harrison. This approach allow us to introduce previously described orthonormal simplifications in the theoretical formalism and still keep the physical character of the tight binding parameters. We would like to turn readers attention on the fact that, in some models the tight binding parameters are considered more like fitting parameters then physical observable. In our opinion, such approach is incorrect, since it do not provide full physical discussion of the electronic states.

In its original form the HTBT model is considered as a transferable method for tetrahedral phases [63]. In particular, the values provided by the classical form of the HTBT, results in only qualitative description of the electronic states for the atomic wires composed of the low lying chemical elements [63]. However, one can put aside the universality of the HTBT approach and adjust these parameters to the experimental or first principle results by varying their values.

In the present work the classical HTBT parameters has been rescaled in order to match the density functional theory results presented in [32], [64]. The values of the TB parameters utilized in our work along with its comparison to the classical values by Harrison are presented in Tab. I. We would like to indicate that in Tab. I both sets of parameters (the classical and re-parametrized ones) have the same relation to the physical quantities. In particular, the binding energies have fixed negative values which are relative to the energy of the electron in isolated hydrogen atom. Additionally we note, that the values of the on-site Hamiltonian matrix elements for states p_x, p_y and p_z are the same and equal $\varepsilon_p^{n,\alpha}$. In contrast to the $\varepsilon_l^{n,\alpha}$ parameters the off-diagonal distance dependent elements are calculated on the basis of Eq.(2) and can be either positive or negative. This situation arises from the fact that one have to require the cohesive character of the interatomic forces. With the reference to this assumption, the interactions between orbitals of the same sign causes overlap of those orbitals to be positive, so the parameter $h_{l,l',m}^{n,n',\beta}$ must be negative. In analogy, negative overlap between orbitals of different signs provide positive value of the off-diagonal elements. The off-diagonal Hamiltonian matrix elements for interactions between s and p-type states are included only between s and p_x orbitals, since interactions between s and p_y or p_z states vanishes in the one-dimensional case in order to the symmetry conditions. Additionally we assume the interactions between p_x states as $h_{p,p,\sigma}^{n,n',\beta}$, while the elements for interactions p_y-p_y and p_z-p_z are equal in energies and assumed as $h_{p,p,\pi}^{n,n',\beta}$.

We note that, except of the p-state binding energy of silicon, all values of the TB parameters proposed in this work are smaller then in its classical form of the Harrison model. One can attribute this fact to the influence of the local environment of the low-coordinate systems, for which the binding energies are usually smaller then in a bulk case. However the value of the p-state binding energy of silicon is somehow greater when compared to the Harrison fit. In our opinion it is due to the lack of the additional high-energy orbitals on the basis set *e.g.* the peripheral Louie-type s^* state [66]. In the case of the nearest-neighbor coupling terms one can notice that the relations between the consecutive parameters for carbon and silicon are identical as in its classical forms. Hence, the physical meaning of these is conserved. Again lower values of the re-parametrized parameters suggest environmental influence.

TABLE I: The values of the tight binding parameters (in eV) and Harrison's fitting coefficients (dimensionless) proposed in this work and compared with the original values by Harrison [63]. Please note that the distance dependent $h_{l,l',\sigma}^{n,n',\beta}$ parameters are computed for the appropriate interatomic spacings d_β (in Å) tabulated below and assumed after [32] and [64].

	Harrison TB parameters			Our TB parameters		
α	C	Si		C	Si	
ε_s	-19.38	-14.79		-18.89	-13.5	
ε_p	-11.07	-7.59		-10.94	-8.38	
β	C	Si	SiC	C	Si	SiC
$\eta_{s,s,\sigma}$	-1.32			-0.93	-1.48	-1.11
$\eta_{s,p,\sigma}$	1.42			0.94	1.19	0.95
$\eta_{p,p,\sigma}$	2.22			1.03	1.18	0.99
$\eta_{p,p,\pi}$	-0.63			-0.59	-0.41	-0.62
β	C	Si	SiC	C	Si	SiC
$h_{s,s,\sigma}$	-5.95	-2.08	-3.70	-4.19	-2.33	-3.11
$h_{s,p,\sigma}$	6.40	2.24	3.98	4.23	1.87	2.66
$h_{p,p,\sigma}$	10.01	3.50	6.22	4.64	1.86	2.77
$h_{p,p,\pi}$	-2.84	-0.99	-1.77	-2.66	-0.65	-1.74
β	C		Si		SiC	
d_β	1.3		2.2		1.649	

The electronic structures of the infinite MLCW, MLSiW, and DLSiCW, obtained using the re-parametrized Harrison tight-binding terms are compared with results computed on the basis of classical HTBT parameters and previously reported DFT calculations in Fig.3. It is also worth to note that in the case of the first two electronic structures (respectively for MLCW and MLSiW wires) we assume only one atom per PUC, whereas the SiC diatomic wires consist of two atoms per PUC. Moreover, the disused band structures are supplemented by the corresponding density of states results. In addition we note that, our tight-binding results are represented by the solid curves whereas the classical HTBT results and DFT bands (after [32], [64]) by open triangles, and dots, respectively. Please note that the re-parametrized tight-binding electronic states are additionally marked by colors due to the proper distinction between their different characters (such convention is assumed for all results in this paper). For first two structures (respectively MLCW and MLSiW nanojuntions) red and blue colors correspond respectively to the σ and σ^* bands. These bands arises from the sp_x orbital hybrids, where the lowest lying bands are always occupied by two electrons. Bands marked by red color has π character and

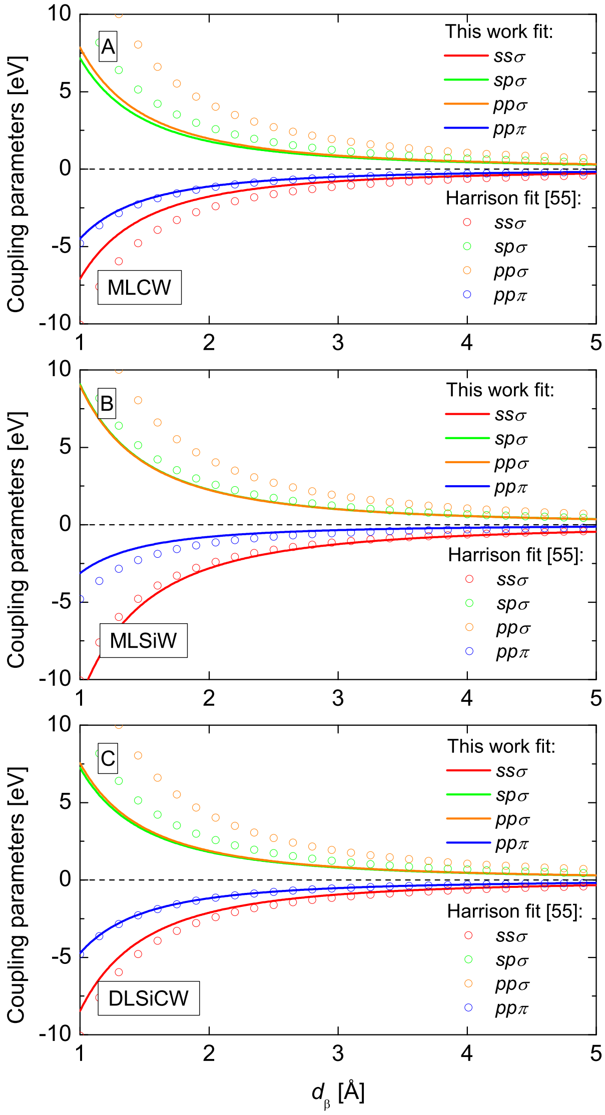

FIG. 2: The nearest-neighbor tight binding coupling parameters as a function of the interatomic distance.

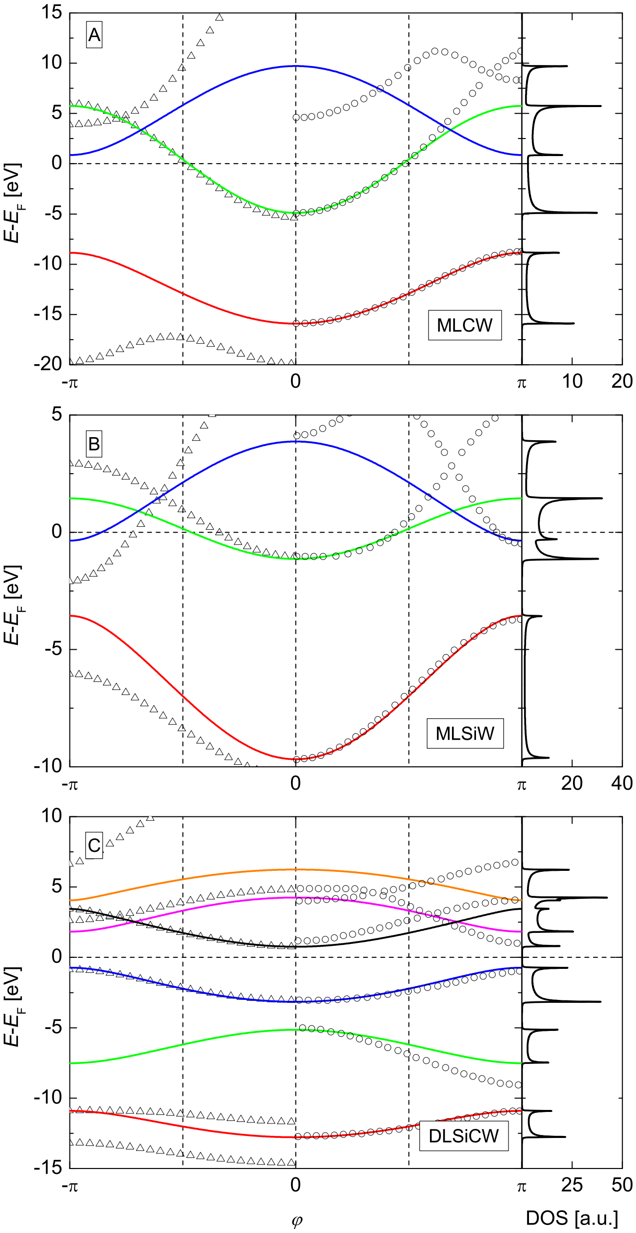

FIG. 3: Electronic structures of carbon (A), silicon (B) and and silicon carbide (C) linear atomic wire nanojunctions, presented over the first Brillouin zone, $ka \in [-\pi, \pi]$. Our results are represented by the solid color curves and compared with the first-principle results (open dots, $ka \in [0, \pi]$) [32], [64], and the tight binding results obtained using the classical parameters by Harrison (open triangles, $ka \in [-\pi, 0]$) [63].

are doubly degenerate. Their origin lays in p_y and p_z orbitals, allows them to hold up to four electrons. For both MLCW and MLSiW structures the π-type bands crosses the Fermi energy level, which means that these atomic wires has purely metallic character. Instead of first two linear wires the electronic structure of the DLSiCW consists of overall eight bands. Starting from the DALSiCC band structure minimum consecutive bands has their origin in the following orbitals: C $3s$ (red band), Si $3s$ (green band), C $3p$ (blue and black bands), and Si $3p$ (pink and orange bands). Additionally for such energy levels order one can notice two doubly degenerate π-type bands, respectively indicated by the blue and orange colors, and an insulating character of DLSiCW.

We would like to turn readers' attention on the fact that stated metallic or insulating characters of the considered atomic wires are appropriate only when the wires are infinite. It is a well known fact that this character can change for the case of finite number of atoms in a given wire or due to the type and quality of connected electron reservoirs.

Furthermore, on the basis of the Fig. 3, one can notice that, for MLCW and MLSiW, the re-parametrized HTBT terms reproduces the DFT result with the quantitative agreement put to the energies slightly above the

Fermi level. Electronic branches in the regions of high-energies are in qualitative agreement. In the case of DL-SiCW some of the electronic states, even in high-energy regions perfectly matches the DFT results. Our parameters in this manner constitute the most optimal set of the parameters for the electronic transport calculations, since it allows us to consider more reasonable energy ranges that the classical HTBT terms, and what is even more important, correctly reproduce the Fermi level.

B. Evanescent states

The electronic structure characteristics for the infinite MLCW, which constitute the electronic leads in our calculations, are additionally supplemented by the numerical results for the generalized eigenvalue problem (10) in two possible representations. The top row of the Fig. (3) presents the three-dimensional representation of the $z(E)$ generalized functional behavior for all electronic states symmetries. Please note, that electronic states with $|z| = 1$ correspond to the propagating waves, whereas the solutions for $|z| < 1$ and $Im[z] = 0$ describe evanescent waves. The moduli of the complex z factors are presented in the bottom row of the Fig. (3). In this case each plate denotes propsgating states, while the evanescent waves are represented by the exponential-like curves. We would like to emphasize the fact that results presented in Fig. (3) provide more complete view on the electronic properties of a given system then a typical band structure representation as in Fig (2), since it represent both propagating and localized states. Such general representation is necessary for the proper discussion of the scattering problem in a disordered systems. In particular, on the basis of Fig.4 (B) one can notice that, as we stated in section I, the evanescent states of given states are always outside the region defined by the propagating waves in this state. However, evanescent solutions to the eigenvalue problem (10) overlap the energy ranges of propagating states of another l-type character. This fact clearly indicate the importance of the evanescent states in the description of electronic transport properties for a nanoscale systems.

In what follows, the energy range considered in our calculations is restricted by the electronic structure boundaries. It creates a energy *window* of physically acceptable solutions. This energy range is marked by two grey vertical lines in Fig.4 (B).

C. Transport properties

In the last step the electronic transport properties of the silicon-doped carbon wire nanojunctions between two semi-infinite one-dimensional carbon leads have been calculated using the PFMT method.

In Fig. (5), the group velocities of electrons in the MLCW perfect leads are presented. It is these group velocities of the electrons incident from the perfect leads, which are used to normalize the scattering matrix. In particular, five different arrangements of the silicon atoms in the nanojunction region have been considered (please see Fig. (6)). The first three represents periodic DLSiCW composed of respectively 1, 2, and 3 Si-C atomic pairs. Next case correspond to the nanojunction wire system composed of 3 carbon and 3 silicon atoms, but without the long range periodic arrangement. Finally, fifth system incorporates 5 silicon atoms and only one carbon atom in the middle.

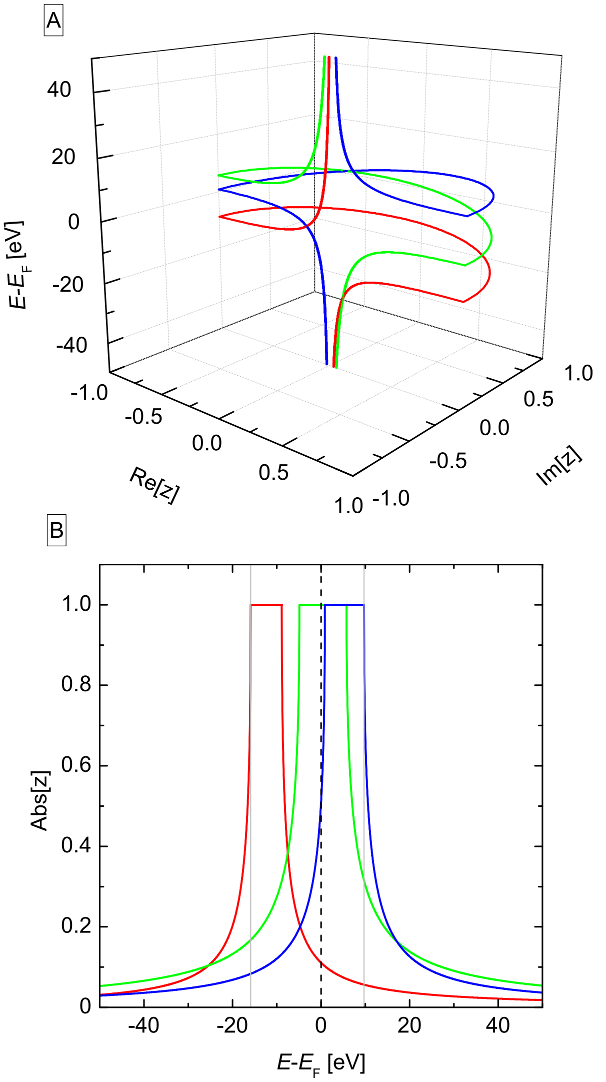

FIG. 4: Three-dimensional representation of the functional behavior $z(E)$ on complex z plane (A) along with the evolution of the absolute value of the complex z factors as a function of the energy E for MLCW (B). Given electronic state symmetries are marked by different colors corresponding to the electronic structure characteristics from Fig. (3). Please note, that the results are presented for the intervals $E = [-50, 50]$ eV and $Im[z] = [0, 1]$) in order to receive transparent representation.

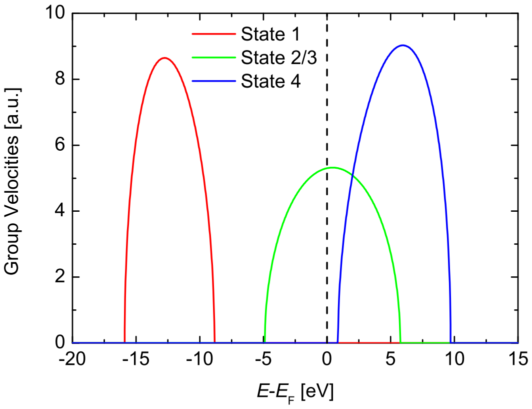

FIG. 5: Group velocities over the intervals of propagating states for MLCW perfect leads.

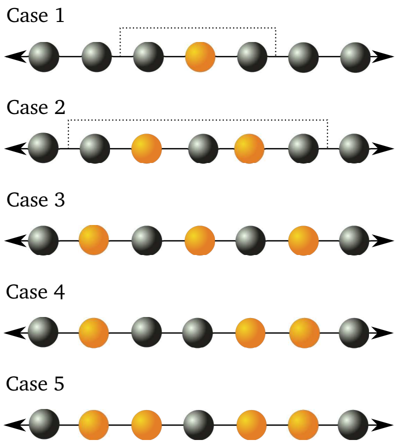

FIG. 6: Schematic representation of the five different arrangement of the silicon and carbon atoms on the nanojunction wire region, which are considered in this section. All presented nanojuctions are assumed to be held between two semi-infinite quasi-onedimensional carbon wires. Here the irreducible region for case 1 and 2 is marked by the dotted lines, whereas for remaining cases only irreducible regions, without lead's atoms, are presented.

The calculated transmission and reflection component scattering cross sections for each of four available transport channels are presented in Fig. (7). Each row of the subfigures correspond to the given considered arrangement of the silicon and carbon atoms on the wire nanojuction *i.e.* case 1 - (A)-(C), case 2 (D)-(F), case 3 (G)-(I), case 4 (J)-(L), and case 5 (M)-(O). The red and green solid lines represent the transmission and reflection component cross sections, respectively. The unitarity condition (light blue lines) is used systematically as a check on the numerical results. Finally, the Fermi level is marked by dashed lines and set as reference at zero energy. Once again we impose the fact that, on the zero bias limit, the total conductance is read at this Fermi level.

On the basis of obtained results we observe that, the transmission spectra presents strongly localized scattering resonances, which number differ depending on the number of silicon atoms on the nanowire. In what follows, valence σ-state (state 1) exhibit small transmission in each of the five considered nanojunctions. Only in the cases 2 and 3 narrow transmission peaks can be noticed. At the zero bias limit the most significant channels are constituted by the degenerate π-type states (state 2 and 3), since only these states crosses the Fermi level. Apart of this fact, also the characteristics of the high-energy states (state 4) may prove to be useful in the discussion of the electronic transport across the silicon-doped carbon wires. In each of the five cases, the transmission around the energy of 5 eV is close to the unit. This fact will be important, when applied bias rise the energy of the incident electrons, allows them to be transmitted at higher, then the Fermi level, energies.

The total conductance of the considered systems has been depicted in Fig. (8), as a function of energy (red solid lines). We note that $G(E)$ is expressed in the G_0 units of the conductance quantum. Furthermore, we have plotted the conductance of the infinite MLCW (solid light blue line) and the Felmi level position (dashed lines). The total conductance spectra directly correspond to the transmission probabilities of the appropriate nanojunction wires presented in Fig. (7). However, since π-type states (states 2 and 3) are degenerate, the value of the $G(E)$ in the energy range of these states is in fact, the summation over these two identical channels. In addition, we notice that, the most significant contribution to the total conductance in the zero bias limit is given by these degenerate π-type states, since only these states of the perfect leads crosses the Fermi level. In particular, for the three first cases which represent the DLSiCW of different lengths, the total conductance at the Fermi level is non-zero. This observation is in contradiction to the insulating character of the infinite DLSiCW. On can connect the non-zero value of the conductance of a short DLSiCW nanojunction wires to the band gap around the Fermi level in the infinite DLSiCW systems (please see Fig. 3 (C)). Further, this band gap is related to the difference between the binding energies of the silicon and carbon atoms, respectively. Mentioned energy difference creates the effective potential barrier for the electron crossing the nanojuction region from left to the right lead. When the wire length is increased the incident electrons encounter periodic repetition of such silicon-carbon potential barriers, and the cumulative effect of the conductance value decrease when the length of the DLSiCW nanojuntion increases, is observed. In our results this effect can be observed both in figures (7) and (8), where the transmission and consecutively total conductance spectra around the Fermi level exhibits minima. These minima are stronger when the wire nanojunctions are longer.

The two remaining silicon-carbon nanojuctions of cases 4 and 5, respectively, are no longer of the periodic types. In the case 4, the number of the silicon atoms on the

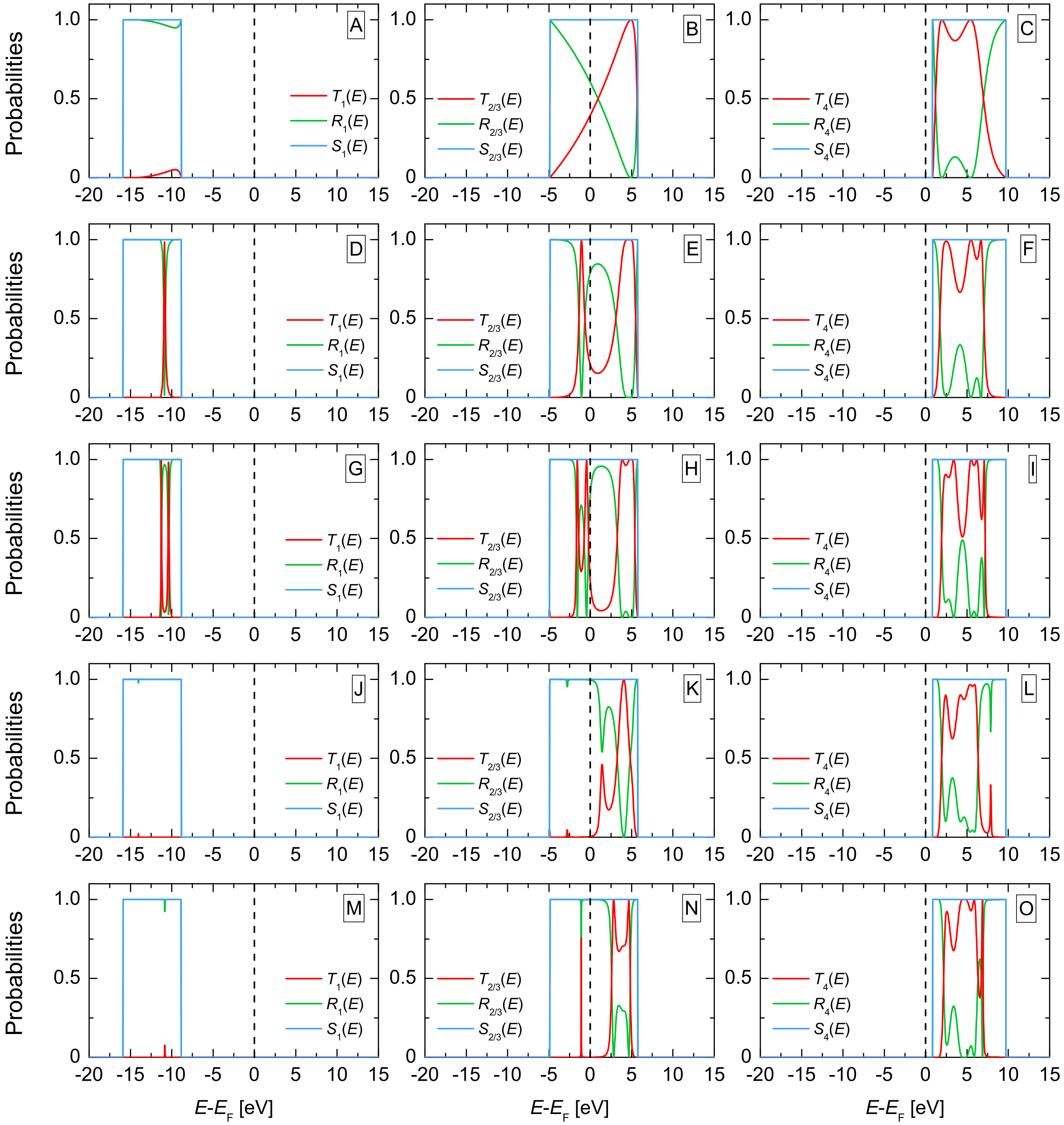

FIG. 7: The transmission and reflection probabilities arcross five considered types of the silicon-doped carbon wires between two semi-infinite one-dimensional carbon leads. The arrangement of the subfigures is following: (A)-(C) - case 1, (D)-(F) - case 2, (G)-(I) - case 3, (J)-(L) - case 4, and (M)-(O) - case 5. The Fermi level is set at the zero energy reference position.

nanowire is the same as in the case 3, however there is no more long range order in the arrangement of the carbon and silicon atoms. Such structural defect, for relatively short wires, completely decreases value of the $G(E)$ at the Femi level to zero. Further, in the fifth case, the number of the silicon atoms outnumber carbon atoms in the nanojunction region. Similarly as in the case of the 4, the total conductance at the Fermi level is zero, however the overall shape to the $G(E)$ spectra is different. I this case the zero value of the conductance is imposed by the large number of the chemical defects constituted by the silicon atoms on the nanojunction wire.

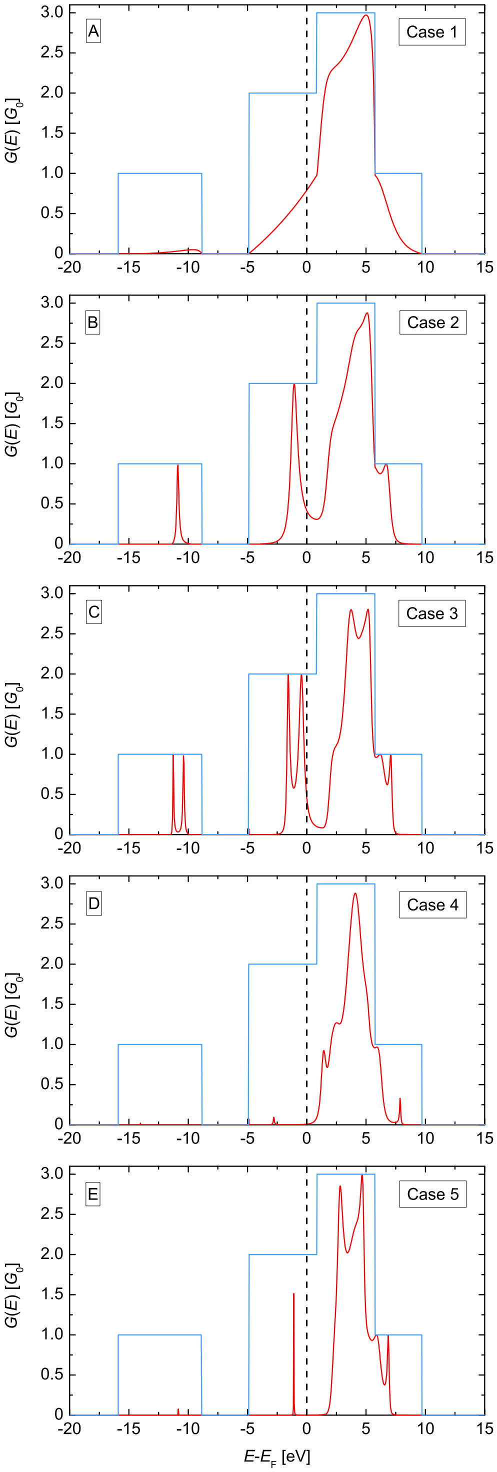

FIG. 8: Total electronic conductance spectra as a function of energy for silicon doped carbon wires (red solid lines). Furthermore, the conductance spectra of the perfect infinite MLCW nanojunction is depicted (light solid lines). Each $G(E)$ function is expressed in the G_0 units, and the Fermi level is set at zero energy reference position (dashed line).

IV. CONCLUSIONS

In the present work, the electronic and transport properties of the silicon-doped carbon wire nanojunctions wires are discussed within the phase field matching theory on the level of the tight-binding approximation. The minimal basis of the atomic wave functions is assumed to be composed of four different atomic orbitals, namely the s, p_x, p_y, and p_z types.

In the first step of our discussion, we present new values of the tight-binding parameters for the prefect infinite carbon (MLCW), silicon (MLSiW), and silicon-carbide (DLSiCW) nanojunction wires, by matching these to the previously reported density functional results. During the fitting procedure we benefit form the Harrion tight-bidning scheme, which allows us to neglect the overlap Hamiltonian terms, and assume the two-center approximation for the Hamiltonian interaction integrals.

Such set of the tight-binding parameters is then used in order to calculate the electronic transport properties of the silicon-doped carbon wire nanojunctions wires. In particular, we consider five different cases of the atoms arrangement on the nanojunction region. We show, that apart of the infinite insulating DLSiCW nanojunctions its finite implementation exhibit a non-zero conductance values. This fact is explained by arguing that the energy difference between the binding energies of the silicon and carbon atoms results in the effective potential barrier for the electron crossing the nanojuction region from left to the right lead. Next we consider the structural defect in the diatomic silicon-carbon arrangement of the atoms on the nanojunction wire. By changing the position of two silicon and carbon atoms we show that the total conductance of the systems drops when comparing to the corresponding periodic configuration of the atoms, resulting in the zero value of the total conductance. In the last step, we present the case when the silicon atoms outnumber the carbon atoms on the nanojunction region. Again, the zero conductance of the system is observed. This is due to the chemical defect influence of the relatively large number of the silicon atoms.

In summary, the PFMT method prove to be useful tool for the quantum transport calculations, and may be considered as a alternative to the non-equlibrium Green's function methods. Furthermore, it is especially interesting for the treatment of complex systems presenting multi-channel conductance, and for the calculation of the conductance properties of nanojuctions which can exhibit electron-phonon interactions with or without chemical and structural defects.

V. ACKNOWLEDGMENTS

One of the authors, D. S., would like to acknowledge his PhD support from the French Ministry of Foreign Affairs (grant CNOUS 2009-2374), the Polish National Science Center (grant DEC-2011/01/N/ST3/04492), and the support of the University of Maine 3MPL Graduate School.

Appendix A: Explicit forms of the $\mathbf{E}_{i,j}$ and $\mathbf{H}_{i,j}$ matrices

On-diagonal ($\mathbf{E}_{i,j}$) and off-diagonal ($\mathbf{H}_{i,j}$) Hamiltonian matrices are in agreement with the following definition of the one-dimensional tight-binding Hamiltonian

$$\begin{aligned} H \; &= \; \sum_{lnN} \epsilon_l^{n,\alpha} \delta_{l,l'} \delta_{n,n} \delta_{N,0} \\ &+ \; h_{l,l',m}^{n,n',\beta} (\delta_{n,n\pm1}\delta_{N,0} + \delta_{n,n\pm1}\delta_{N,N\pm1}), \end{aligned} \tag{A1}$$

where symbol δ denotes Kronecker delta. Analogically to the Eq. (1), Hamiltonian (A1) is defined for general case of overall N_x atoms in unit cell and N_l different orbitals per atom. After Eq. (A1), the general explicit form of $\mathbf{E}_{i,j}$ matrix is given by

$$\mathbf{E}_{i,j} = \begin{pmatrix} \boldsymbol{\varepsilon}_1 & \mathbf{h}_{2,1}^{\dagger} & \cdots & \cdots & \mathbf{h}_{n,1}^{\dagger} \\ \mathbf{h}_{2,1} & \boldsymbol{\varepsilon}_2 & \ddots & & \vdots \\ \vdots & \ddots & \ddots & \ddots & \vdots \\ \vdots & & \ddots & \boldsymbol{\varepsilon}_{n-1} & \mathbf{h}_{n,n-1}^{\dagger} \\ \mathbf{h}_{n,1} & \cdots & \cdots & \mathbf{h}_{n,n-1} & \boldsymbol{\varepsilon}_n \end{pmatrix}, \tag{A2}$$

while matrix $\mathbf{H}_{i,j}$ by

$$\mathbf{H}_{i,j} = \begin{pmatrix} 0 & \cdots & \mathbf{h}_{1,2} & \cdots & \mathbf{h}_{1,n-1} & \mathbf{h}_{1,n} \\ \vdots & \ddots & \ddots & \ddots & \mathbf{h}_{2,n-1} & \mathbf{h}_{2,n} \\ 0 & \ddots & \ddots & \ddots & \ddots & \vdots \\ \vdots & \ddots & \ddots & \ddots & \ddots & \mathbf{h}_{n,n} \\ 0 & 0 & \ddots & \ddots & \ddots & \vdots \\ 0 & 0 & \cdots & 0 & \cdots & 0 \end{pmatrix}, \tag{A3}$$

where

$$\boldsymbol{\varepsilon}_{i',j'} = \begin{pmatrix} \varepsilon_s^{n,\alpha} & 0 & \cdots & \cdots & 0 \\ 0 & \varepsilon_{p_x}^{n,\alpha} & \ddots & & \vdots \\ \vdots & \ddots & \ddots & \ddots & \vdots \\ \vdots & & \ddots & \varepsilon_{l-1}^{n,\alpha} & 0 \\ 0 & \cdots & \cdots & 0 & \varepsilon_l^{n,\alpha} \end{pmatrix}, \tag{A4}$$

and

$$\mathbf{h}_{i',j'} = \begin{pmatrix} h_{s,s,\sigma}^{n,n',\beta} & h_{s,p_x,\sigma}^{n,n',\beta} & \cdots & \cdots & h_{s,l',m}^{n,n',\beta} \\ h_{p_x,s,\sigma}^{n,n',\beta} & h_{p_x,p_x,\sigma}^{n,n',\beta} & \ddots & & \vdots \\ \vdots & \ddots & \ddots & \ddots & \vdots \\ \vdots & & \ddots & h_{l-1,l'-1,m}^{n,n',\beta} & h_{l-1,l',m}^{n,n',\beta} \\ h_{l,s,m}^{n,n',\beta} & \cdots & \cdots & h_{l,l'-1,m}^{n,n',\beta} & h_{l,l',m}^{n,n',\beta} \end{pmatrix}. \tag{A5}$$

Both Eq. (A2) and (A3) denotes $N_x N_l$ square matrices, where matrix (A3) is upper triangular. In this manner component matrices (A4) and (A5) are of the dimension $N_l \times N_l$. Additionally, matrix $\boldsymbol{\varepsilon}_{i',j'}$ always denotes diagonal matrix, while $\mathbf{h}_{i',j'}$ matrix is much more complex, with possible non-zero elements at every position. Please note, that some of the $h_{l,l',m}^{n,n',\beta}$ elements can vanish due to the symmetry conditions and simplifies the notation of the $\mathbf{h}_{i',j'}$ matrix.

Appendix B: Partitioning technique

The partitioning technique is suitable method which allows to avoid singularity problem of the $\mathbf{H}_{N,N-1}$ and $\mathbf{H}_{N,N-1}^{\dagger}$ matrices and calculate only non-trivial solutions of eigenvalue problem (10). Detail discussion of the partitioning technique is presented in [65] and this section gives only our short remarks on this method.

Following studies from [65] problem (10) is partitioned into two parts, of respectively $D_1 - D_2$ and D_2 sizes, where

$$D_1 = N_x N_l, \tag{B1}$$

and

$$D_2 = N_n N_l. \tag{B2}$$

In Eq. (B2), parameter N_n stands for the order of nearest-neighbour interactions assumed in calculations *e.g.* $N_n = 1$ for the first nearest-neighbour interactions. on the basis of Eq. (B1) and (B2), reduced $2N_l$ eigenvalue problem is written as

$$\begin{aligned} &\left[\begin{pmatrix} \mathbf{A}_{1,1} & \mathbf{A}_{1,2} \\ \mathbf{I}_{2,2} & 0 \end{pmatrix} - z \begin{pmatrix} \mathbf{B}_{1,1} & \mathbf{B}_{1,2} \\ 0 & \mathbf{I}_{2,2} \end{pmatrix} \right] \\ &\times \begin{pmatrix} \mathbf{c}_2(x_N, \mathbf{k}) \\ \mathbf{c}_2(x_{N-1}, \mathbf{k}) \end{pmatrix} = 0. \end{aligned} \tag{B3}$$

At this point we correct the misprint from [65] and write the submatrices of Eq. (B3) in the following form

$$\mathbf{A}_{1,1} = E\mathbf{I}_{2,2} - \mathbf{E}_{2,2} - \mathbf{E}_{2,1} \left(E\mathbf{I}_{1,1} - \mathbf{E}_{1,1} \right)^{-1} \mathbf{E}_{1,2}, \tag{B4}$$

$$\mathbf{A}_{1,2} = -\mathbf{H}_{2,2} - \mathbf{E}_{2,1} \left(E\mathbf{I}_{1,1} - \mathbf{E}_{1,1} \right)^{-1} \mathbf{H}_{1,2}, \tag{B5}$$

$$\mathbf{B}_{1,1} = \mathbf{H}_{2,2}^{\dagger} + \mathbf{H}_{1,2}^{\dagger} \left(E\mathbf{I}_{1,1} - \mathbf{E}_{1,1} \right)^{-1} \mathbf{E}_{1,2}, \tag{B6}$$

$$\mathbf{B}_{1,2} = \mathbf{H}_{1,2} \left(E\mathbf{I}_{1,1} - \mathbf{E}_{1,1} \right)^{-1} \mathbf{H}_{1,2} \tag{B7}$$

Please note, that reduced problem (B3) gives $2N_l$ eigenvalues with $2N_l$ corresponding eigenvectors, what is N_x times less then can be expect from the physical point of view. Nevertheless, those solutions can be easily separated into $N_x N_l$ eigenvalues and $N_x N_l$ eigenvectors of a purely physical character.

Appendix C: Explicit forms of the $\mathbf{M}_{i,j}$, $\mathbf{M}_1^{in}$, and $\mathbf{M}_2^{in}$ components

The sub-matrices of the equation (18), for a given i and j indices, are given as

$$\mathbf{M}_{i,j} = \mathbf{E}_i \;\text{ for }\; \begin{cases} i = j \\ N > i > 1 \\ N > j > 1 \end{cases}, \tag{C1}$$

$$\mathbf{M}_{i,j} = -\mathbf{H}_{i,i-1} \;\text{ for }\; \begin{cases} i \neq j \\ i > 2 \\ j = i - 1 \end{cases}, \tag{C2}$$

$$\mathbf{M}_{i,j} = -\mathbf{H}^{\dagger}_{i,i-1} \;\text{ for }\; \begin{cases} i \neq j \\ i < N - 2 \\ j = i + 1 \end{cases}, \tag{C3}$$

except of the sub-matrices which describe the boundary atoms of the system and are expressed in the following manner

$$\begin{aligned} &\mathbf{M}_{1,1} = \mathbf{H}^{\dagger}_{-N+3,-N+2}\mathbf{c}_{l'}(\mathbf{k})z, \\ &\mathbf{M}_{2,1} = -\mathbf{H}_{-N+4,-N+3}\mathbf{c}_{l'}(\mathbf{k})z^{N-3}, \\ &\mathbf{M}_{N-1,N} = -\mathbf{H}^{\dagger}_{N-4,N-5}\mathbf{c}_{l'}(\mathbf{k})z^{N-3}, \\ &\mathbf{M}_{N,N} = \mathbf{H}_{N-3,N-4}\mathbf{c}_{l'}(\mathbf{k})z. \end{aligned} \tag{C4}$$

Finally, the $\mathbf{M}_1^{in}$ and $\mathbf{M}_2^{in}$ vector components are written as

$$\mathbf{M}_1^{in} = \mathbf{H}^{\dagger}_{-N+3,-N+2}\mathbf{c}_{l}(\mathbf{k})z^{N-4}, \tag{C5}$$

and

$$\mathbf{M}_2^{in} = -\mathbf{H}_{-N+4,-N+3}\mathbf{c}_{l}(\mathbf{k})z^{-N+3}. \tag{C6}$$

Appendix D: Group velocities

As specified in section II C, the group velocities for individual states, can be calculated on the basis of eigenvalue problem (6) rewritten in the following manner

$$[v\mathbf{I} - \mathbf{V}]\,\mathbf{v}(x_N, \mathbf{k}) = 0, \tag{D1}$$

where v denotes the eigenvalues of Eq. (D1) which yields all required electron group velocities for each propagating state. Further $\mathbf{V}$ is the $N_x \times N_l$ size matrix of the form

$$\mathbf{V} = \frac{\partial\tilde{\mathbf{H}}}{\partial\mathbf{k}}. \tag{D2}$$

Finally $\mathbf{v}(x_N, \mathbf{k})$ stands for eigenvectors of problem (D1). We note that usually equation (D2) includes the constant part d_β/h, where h is the Planck constant. However, for the purpose of electronic transport calculations within the PFMT approach, this term can be omitted due to the fact that only the ratios of the given group velocities are important (please see Eq. (21) and Eq. (22)).

Appendix E: Density of states and Fermi energy

In order to calculate the density of states for a given system we define the retarded matrix Green's function of the form

$$G(E, \mathbf{k}) = [(E + i\zeta)\mathbf{I} - \tilde{\mathbf{H}}]^{-1}, \tag{E1}$$

using the typical mathematical trick *i.e.* adding small imaginary part $i\zeta$ to the energy E. Next, the total density of states can be calculated on the basis of the following relation

$$\mathrm{DOS}(E) = \int_0^{\pi} \mathrm{Im}[\mathrm{Tr}[G(E, \mathbf{k})]]. \tag{E2}$$

The partial DOS is then simply calculated on the basis of general equations (E1), and (E3), for a given eigenvalue.

In what follows, the Fermi energy for a given system is determined on the basis of carrier concentration calculations. Assuming total N_e electrons per atom, the total carrier concentration

$$\mathrm{C} = \int_{E_{min}}^{E_{max}} \int_0^{\pi} \mathrm{Im}[\mathrm{Tr}[G(E, \mathbf{k})]], \tag{E3}$$

is computed in the energy range from the band minimum E_{min} to the band maximum E_{max}. Similarly to density one states Eq.(E3) serve also as a basis for the calculations of partial carrier concentration values for a given electronic state.

Now, the carrier concentration of the lowest state occupied by the $N_{e'}$ atoms can be calculated, to be next multiplied by the number $N_e/N_{e'}$, and give the C_T carrier concentration of the total N_e electrons per atom. Finally if C in Eq. (E3) is set to be equal to C_T the E_{max} is obviously the Fermi energy.

---

[1] K.S. Novoselov, A.K. Geim, and S.V. Morozov, Science 306 (2004) 666-669.

[2] A.K. Geim, K.S. Novoselov, Nature Mater. 6 (2007) 183-191.

[3] H.W. Kroto, J.R. Heath, S.C. O'Brien, R.F. Curl and R.E. Smalley, Nature 318 (1985) 162-163.

[4] S. Iijima, Nature 354 (1991) 56-58.

[5] S. Iijima, T. Ichihashi, Nature 363 (1993) 603-605.

[6] P.L. Euen, Nature 393 (1998) 15-16.

[7] C. Jin, H. Lan, L. Peng, K. Suenaga, and S. Iijima, Phys. Rev. Lett. 102 (2009) 205501.

[8] J.R. Heath, Q. Zhang, S.C. O'Brien, R.F. Curl, H.W. Kroto, and R.E. Smalley, J. Am. Chem. Soc. 109 (1987) 359-363.

[9] R.J. Lagow, J.J. Kampa, H.C. Wei, S.L. Battle, J.W. Genge, D.A. Laude, C.J. Harper, R. Bau, R.C. Stevens, J.F. Haw, and E. Munson, Science 267 (1995) 362-367.

[10] V. Derycke, P. Soukiassian, A. Mayne, G. Dujardin, and J. Gautier, Phys. Rev. Lett. 81 (1998) 58685871.

[11] H.E. Troiani, M. Miki-Yoshida, G.A. Camacho-Bragado, M.A.L. Marques, A. Rubio, J.A. Ascencio, and M. Jose-Yacaman, Nano Lett. 3 (2003) 751-755.

[12] X. Zhao, Y. Ando, Y. Liu, M. Jinno, and T. Suzuki, Phys. Rev. Lett. 90 (2003) 187401.

[13] T.D. Yuzvinsky, W. Mickelson, S. Aloni, G.E. Begtrup, A. Kis, and A. Zettl, Nano Lett. 6 (2006) 2718-2722.

[14] A. Nitzan and M.A. Ratner, Science 300 (2003) 1384-1389.

[15] C.C. Wan, J.L. Mozos, G. Taraschi, J. Wang, and H. Guo, Appl. Phys. Lett. 71 (1997) 419-421.

[16] J.L. Mozos, C.C. Wan, J. Wang, and H. Guo, Phys. Rev. B 56 (1997) 4351-4354.

[17] G. Taraschi, J.L. Mozos, C.C. Wan, H. Guo, and J. Wang, Phys. Rev. B 58 (1998) 13138-13145.

[18] M. Kértesz, J. Koller, and A. Ažman, J. Chem. Phys. 68 (1978) 2779-2782.

[19] M. Kértesz, J. Koller, and A. Ažman, Phys. Rev. B 19 (1979) 2034-2040.

[20] A. Karpfen, J. Phys. C: Solid State Phys. 12 (1979) 3227-3237.

[21] M. Teramae, T. Yamabe, and A. Imamura, Theor. Chim. Acta 64 (1983) 1-12.

[22] M. Springborg, J. Phys. C: Solid State Phys. 19 (1986) 4473-4482.

[23] M.J. Rice, S.R. Phillpot, A.R. Bishop, and D.K. Campbell, Phys. Rev. B 34 (1986) 4139-4149.

[24] M. Springborg, S.L. Dreschel, and J. Málek, Phys. Rev. B 41 (1990) 11954-11966.

[25] J.D. Watts and R.J. Bartlett, J. Chem. Phys. 97 (1992) 3445-3457.

[26] C.H. Xu, C.Z. Wang, C.T. Chan, and K.M. Ho, J. Phys.: Condens. Matter 4 (1992) 6047-6054.

[27] L. Lou and P. Nordlander, Phys. Rev. B 54 (1996) 16659-16662.

[28] R.O. Jones and G. Seifert, Phys. Rev. Lett. 79 (1997) 443-446.

[29] P. Fuentealba, Phys. Rev. A 58 (1998) 4232-4234.

[30] A. Abdurahman, A. Shukla, and M. Dolg, Phys. Rev. B 65 (2002) 115106.

[31] S. Cahangirov, M. Topsakal, and S. Ciraci, Phys. Rev. B 82 (2010) 195444.

[32] S. Tongay, E. Durgun, and S. Ciraci, Appl. Phys. Lett. 85 (2004) 6179-6181.

[33] E.J. Bylaska, J.H. Weare, and R. Kawai, Phys. Rev. B 58 (1998) R7488-R7491.

[34] Y. Zhang, Y. Su, L. Wang, E. S-W Kong, X Chen and Y Zhang, Nanoscale Res. Lett. 6 (2011) 577.

[35] N.D. Lang and Ph. Avouris, Phys. Rev. Lett. 81 (1998) 3515-3518.

[36] N.D. Lang and Ph. Avouris, Phys. Rev. Lett. 84 (2000) 358-361.

[37] B. Larade, J. Taylor, H. Mehrez, and H. Guo, Phys. Rev. B 64 (2001) 075420.

[38] S. Tongay, S. Dag, E. Durgun, R.T. Senger, and S. Ciraci, J. Phys.: Cond. Matter 17 (2005) 3823-3836.

[39] R.T. Senger, S. Tongay, E. Durgun, and S. Ciraci, Phys. Rev. B 72 (2005) 075419.

[40] Ž. Crljen and G. Baranović, Phys. Rev. Lett. 98 (2007) 116801.

[41] S. Okano and D. Tománek, Phys. Rev. B 75 (2007) 195409.

[42] W. Chen, A.V. Andreev and G.F. Bertsch, Phys. Rev. B 80 (2009) 085410.

[43] Y. Wang, Z-Z Lin, W. Zhang, J. Zhuang, and X-J Ning, Phys. Rev. B 80 (2009) 233403.

[44] B. Song, S. Sanvito, and H. Fang, New J. Phys. 12 (2010) 103017.

[45] G.P. Zhang, X.W. Fang, Y.X. Yao, C.Z. Wang, Z.J. Ding, and K.M. Ho, J. Phys.: Cond. Matt. 23 (2011) 025302.

[46] A.I. Yanson, G.R. Bolliger, H.E. van der Brom, N. Agraït, and J.M. van Ruitenbeek, Nature 395 (1998) 783-785.

[47] Y. Ke, K. Xia and H. Guo, Phys. Rev. Lett. 100 (2008) 166805.

[48] Z. Qiao, J. Wang, Q. Sun, and H. Guo, Phys. Rev. B 79 (2009) 205308.

[49] D. Nozaki, H.M. Pastawski, and G. Cuniberti, New J. Phys. 12 (2010) 063004.

[50] K. Xia, P.J. Kelly, G.E.W. Bauer, I. Turek, J. Kurdnovský, and V. Drchal, Phys. Rev. B 63 (2001) 064407.

[51] K. Xia, P.J. Kelly, G.E.W. Bauer, A. Braatas, and I. Turek, Phys. Rev. B 65 (2002) 220401(R).

[52] K. Xia, P.J. Kelly, G.E.W. Bauer, and I. Turek, Phys. Rev. Lett. 89 (2002) 166603.

[53] M. Zwierzycki, K. Xia, P.J. Kelly, G.E.W. Bauer, and I. Turek, Phys. Rev. B 67 (2003) 092401.

[54] C. Caroli, R. Combescot, P. Nozières, and D. Saint-James, J. Phys. C 8 (1971) 916-929.

[55] P.A. Khomyakov, G. Brocks, V. Karpan, M. Zwierzycki, and P.J. Kelly, Phys. Rev. B 72 (2005) 035450.

[56] a) D. Szczęśniak, A. Khater, R. Szczęśniak, and Z. Bąk, in *Solid State Physics in Modern Materials Research*, edited by K. Dziliński and J.J. Wysłocki (CUT Publishing House, Czestochowa, 2010), pp. 161-173.
b) A. Khater and D. Szczęśniak, J. Phys.: Conf. Ser. **289**, 012013 (2011).

[57] D. Szczęśniak and A. Khater, Eur. Phys. J. B, (2012) doi: 10.1140/epjb/e2012-21055-x.

[58] For a discussion of the matching method for the transport of phonons we refer to:
a) J. Szeftel and A. Khater, J. Phys. C: Solid State Phys. 20 (1987) 4725.
b) Y. Pennec and A. Khater, Surf. Sci. Lett. 348, (1995) L82.
c) A. Fellay, F. Gagel, K. Maschke, A. Virlouvet, and A. Khater, Phys. Rev. B 55 (1997) 1707.
d) A. Khater and M. Belhadi, Surf. Rev. Lett. 16, (2009) 271.
e) B. Bourahla, O. Nafa, and R. Tigrine, Physica B 406 (2011) 725-730.

while for the transport of magnons to:
a) M. Abou Ghantous and A. Khater, Eur. Phys. J. B 12, (1999) 335.
b) B. Bourahla, A. Khater, R. Tigrine, O. Rafil, and M. Abou Ghantous, J. Phys.: Cond. Matt. 19 (2007) 266208.
c) R. Tigrine, A. Khater, B. Bourahla, M. Abou Ghantous, and O. Rafil, Eur. Phys. J. B 62, (2008) 59.

[59] H. Rabani and M. Mardaani, Solid State Commun. **152**, 235-239 (2012).

[60] Y. Wu and P.A. Childs, Nanoscale Res. Lett. **6**, 62 (2011).

[61] J. Chen, L. Yang, H. Yang, and J. Dong, Phys. Lett. A **316**, 101-106 (2003).

[62] J.C. Slater, G.F. Koster, Phys. Rev. 94 (1954) 1498-1524.

[63] W.A. Harrison, Elementary Electronic Structure, second ed., World Scientific, Singapore, 2004.

[64] E. Bekaroglu, M. Topsakal, S. Cahangirov, and S. Ciraci, Phys. Rev. B 81 (2010) 075433.

[65] P.A. Khomyakov and G. Brocks, Phys. Rev. B 70 (2004) 195402.

[66] W.A. Harrison, Phys. Rev. B **24** (1981) 5935-5843.